Robotics: Science and Systems 2026
Sydney, Australia, July 13–17, 2026

A Super-Resolution and Multi-Axis Tactile Sensor with Soft Artificial Skin

Hongxu Wei[1,2], Zhou Lu[1,3], Peisen Xu[1], Yang Xu[1],
Xuanyi Yang[1], Wei Zhao[2], Jiming Chen[1], Gaofeng Li[1*]
[1]Zhejiang University, [2]Northeastern University, [3]Zhejiang University of Technology

***Abstract*—To achieve human-like skin tactile perception with super-resolution, the method of introducing a soft layer on sensing array has attracted increasing attention. Due to the limitations of sensing units principle, most existing tactile sensors can only sense normal force. However, multi-dimensional force information is important for robot manipulation. To address this, we propose a tactile sensing unit based on a tiny monolithic tri-cantilever structure that decouples three-dimensional force. A reconstruction algorithm combined both model-based and learning-based approaches is then proposed to detect the three-dimensional force applied to the sensing unit. These units are arranged in an array and covered with a soft silicone layer which induces traction-coupling effects. By leveraging deep learning, our tactile sensor can estimate the magnitude and position of external three-dimensional force with super-resolution. Experiments have shown that our tactile sensor achieves a Mean Absolute Error (MAE) of 0.19 N for three-dimensional force estimation and 0.49 mm for contact localization. Notably, this corresponds to a 26-fold improvement in spatial resolution, surpassing the state-of-the-art literature. Then the benefits and potential applications of our proposed sensors are validated in several tasks, including the teleoperative transfer of a test tube into a rack and stable robotic grasping under external interference. These demonstrate the practicality of our design and provide new solutions for tactile sensors.**

I. Introduction

Tactile sensing plays an important role in enabling robotic systems to physically interact with complex external environments[1][2]. Unlike visual perception, tactile sensing provides rich local contact information, including contact forces, object shape, surface texture, roughness, as well as material properties such as hardness and temperature[3]. Such information is essential for robust manipulation, allowing robots to perform adaptive grasping and manipulation tasks under uncertainty.

Researchers have explored various tactile sensing methods, which can be broadly categorized into three groups: vision-based tactile sensors (VBTS), array-based tactile sensors without super-resolution capability, and array-based tactile sensors with super-resolution capability. In recent years, VBTS have attracted significant attention[4, 5, 6]. These sensors use cameras to capture the deformation of markers embedded in a soft elastomer, converting tactile stimuli into visual signals. They are renowned for their high spatial resolution and capability to capture rich surface texture details; however, they typically suffer from bulky designs and difficulties in scaling to large sensing areas. To achieve large-area tactile perception, assembling tactile pixels (taxels) into arrays has become a

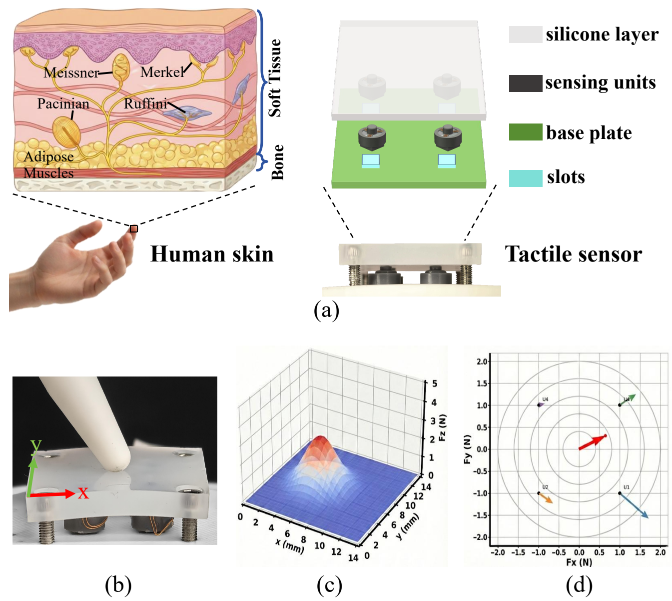

Fig. 1. **Design concept and validation of the proposed tactile sensor.** (a) Structural analogy between human skin and the proposed tactile sensor, where the silicone layer, sensing units, and base plate mimic the mechanical roles of the soft tissue, mechanoreceptors, and bone, respectively. (b) The physical prototype undergoing indentation experiments. (c) Visualization of the super-resolution contact localization and normal force distribution. (d) Resultant shear force vector alongside four sensing units' individual shear force components.

natural solution. Ordinary array-based tactile sensors consist of multiple taxels arranged in an array, whose tactile sensing resolution is fundamentally limited to the physical resolution of the taxel array.

Although increasing array density is a common strategy to enhance resolution, this approach inevitably incurs significant overhead in terms of power consumption, fabrication cost, and hardware complexity. To address these limitations, current research aims to infer dense tactile signals from limited measurements and to generate high-resolution virtual taxels. As a result, array-based tactile sensors with super-resolution capability have emerged as an active research topic.

Despite recent advances, robotic tactile sensors still fall short of human skin, which achieves rich perception through compliant tissue and specialized mechanoreceptors (Pacinian, Meissner's, Merkel's, and Ruffini)[7]. While all of these receptors transduce mechanical stimuli into neural signals, they exhibit substantial differences in adaptation speed, receptive field size, and Mechanical sensitivity, thereby supporting distinct tactile functions. For example, Pacinian corpuscles typically possess large receptive fields and are located in deeper layers of the skin, making them well suited for sensing normal pressure[8]. Importantly, when external forces act on the skin surface, the resulting deformation propagates through the soft tissue. Owing to the traction-coupling effect within the compliant tissue, humans are able to discriminate spatial details smaller than the receptive field size of individual mechanoreceptors, a phenomenon known as super-resolution[9].

Super-resolution sensing is crucial for precise force estimation in tactile sensors. Without super-resolution capabilities, high-resolution tactile sensing can only be achieved by densely packing sensing units, which requires more complex wiring and increases system cost. However, most existing tactile sensors capable of super-resolution primarily detect normal forces[10, 11, 12]. Critically, tangential force information is equally indispensable for robotic manipulation. For example, stable and adaptive grasping tasks heavily rely on the detection of tangential forces[13]. However, simultaneously achieving super-resolution and three-dimensional force sensing remains a significant challenge, primarily due to the complex mechanical coupling under multi-dimensional loads. The overlapping deformation fields often result in severe signal crosstalk, making it difficult to decouple shear forces from normal pressure at sub-taxel resolutions.

In this paper, we introduce a super-resolution three-dimensional force sensing tactile sensor, which overcomes the inherent limitations of ordinary tactile sensors. Compared to existing work, our contributions are summarized as follows:

- **A monolithic Tri-Cantilever 3D Force Tactile Sensing Unit**: We design a tiny monolithic tri-cantilever structure ($\phi\, 8 \times 6.5\,\mathrm{mm}$) sensing unit capable of three-dimensional force estimation. It achieves three-dimensional force decoupling within a compact size, establishing a structural foundation for the scalable deployment of 3D tactile arrays.
- **A Hybrid Model-Learning Framework for 3D Force Sensing**: We propose a hybrid force decoupling strategy that integrates model-based with learning-based approaches to achieve accurate 3D force reconstruction for sensing unit. It achieves superior decoupling accuracy across the full measurement range compared to purely model-based and learning-based methods.
- **Super-Resolution 3D Force Perception via Deep Learning**: The proposed sensor comprises a 2×2 sensing array covered by a compliant silicone layer, which facilitates super-resolution 3D force perception through deep learning reconstruction. To the best of our knowledge, this is the first study to achieve super-resolution 3D force sensing by leveraging individual 3D force sensing units, providing a new approach to tactile sensor design.
- **Performance Evaluation & Task-Level Demonstrations**: Through a series of experiments, we validate that the MAE of the proposed tactile sensor for three-dimensional force and contact localization are $0.19\,\mathrm{N}$ and $0.49\,\mathrm{mm}$, respectively. We verify its effectiveness in a real-world operating scenario by mounting the proposed tactile sensor on the robot gripper to grasp objects. It is able to maintain stable gripping under external disturbances, demonstrating that the sensor can provide reliable three-dimensional force information.

II. RELATED WORK

A. Vision-based Tactile Sensors

VBTS have developed rapidly in recent years[14]. These sensors typically incorporate visual markers, such as dot patterns, embedded within a soft elastomer. When the elastomer comes into contact with the environment, external forces induce surface deformation, which leads to the displacement of the embedded markers in the captured images. By monitoring these deformations with a camera, tactile signals are transformed into visual representations. Contact information is then inferred by analytical modeling or data-driven learning from the resulting images.

A key advantage of VBTS is their high sensing accuracy[15][16]. In particular, they are able to capture rich surface texture information of contacted objects. This capability has enabled a wide range of applications in robotic tactile perception. For instance, Zhang et al. [5] proposed a stereo vision–based tactile sensor (GelStereo 2.0) that explicitly modeled refractive geometry across multiple media, enabling accurate 3D reconstruction of contact geometry. The proposed multi-medium refractive stereo calibration significantly improved depth reconstruction accuracy.

However, they are difficult to scale to large-area sensing, and their sensor modules are typically thick. Due to the reliance on cameras and necessary optical paths, miniaturization remains a significant hurdle. Several studies have attempted to address this issue. ThinTact utilized a lensless imaging technique and significantly reduced the sensor thickness to 9.6 mm while maintaining high-resolution tactile sensing[6]. However, the miniaturization challenge of VBTS has not been fundamentally resolved, and their thickness remains difficult to match with other types of tactile sensors.

B. Array-based Tactile Sensors without Super-resolution Capability

For sensors lacking super-resolution capabilities, the only way to improve the resolution of these sensors is by increasing the physical density of taxels. Each taxel independently measures local mechanical signals and transmits them to the system. By processing these spatially distributed signals, the system reconstructs the contact interface to infer critical information, including object shape, force distribution, and contact states.

However, this reliance on physical density presents a significant bottleneck. Scaling up the number of taxels to achieve high resolution inevitably leads to a dramatic increase in wiring complexity and power consumption. These challenges

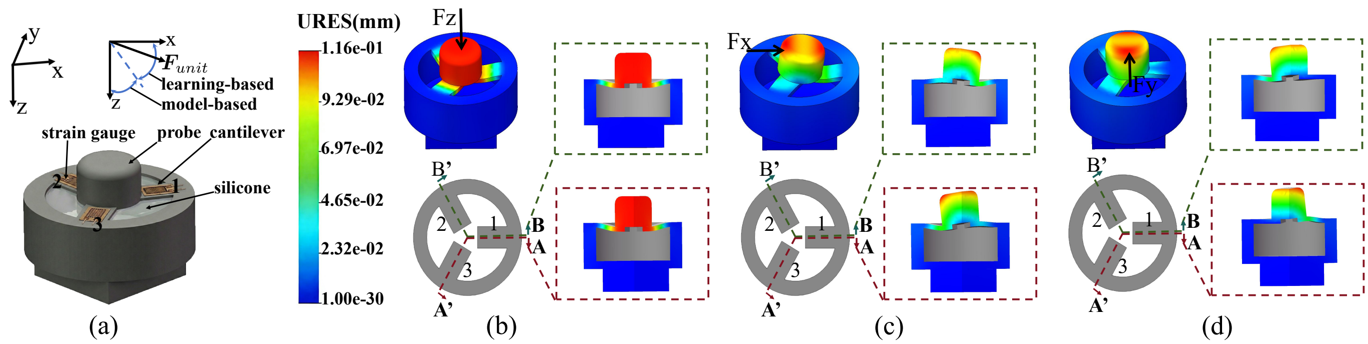

Fig. 2. **Structural configuration and deformation characteristics of the sensing unit.** (a) Sensing unit structure diagram with three cantilevers. (b–d) Finite Element Analysis (FEA) results illustrating the cross-sectional deformations of the cantilevers under: (b) normal force F_z, (c) shear force F_x, and (d) shear force F_y.

become particularly acute when attempting to achieve large-area coverage. For example, Zhao et al. [17] developed a large-scale integrated pressure sensor array covering a 4-inch area with 64×64 taxels. Although achieving a spatial resolution of 0.9 mm, the substantial data bandwidth imposes challenges for real-time processing on embedded controllers. In a different approach, the sensor presented by Wang et al. [18] consists of a 3×3 array of sensing units uniformly distributed on a 12×12 mm substrate. Every sensing unit can measure three-dimensional forces, but the resolution is limited to 3.5 mm due to the low sensor density. Consequently, achieving high spatial resolution with low taxel density remains unfeasible using conventional discrete arrays.

C. Array-based Tactile Sensors with Super-resolution Capability

To balance low sensor density and high spatial resolution, many recent works adopt super-resolution perception. Super-resolution aims to reconstruct high-resolution tactile information from limited or sparse sensor observations using computational methods, thereby overcoming the physical constraints of sensor resolution and quantity. Super-resolution tactile sensor arrays significantly reduce hardware complexity while improving spatial resolution.

However, most existing super-resolution tactile sensing approaches are limited to normal force perception [19, 11, 12, 20]. For instance, Thomas et al. [20] employed 15 barometric sensors arranged in an array covered by an elastomer layer, employing 2D Gaussian model to estimate super-resolution force. Similarly, Kong et al. [19] used model prediction methods to reconstruct normal pressure distributions, achieving spatial resolution beyond the physical spacing between sensing units.

Since real-world physical interactions typically involve both normal and tangential force components, which jointly determine the stability of the interaction. Tangential force information is critical, especially in tasks such as grasping and rotating, where detecting incipient slip is essential[21]. However, simultaneously achieving super-resolution and multi-axis force sensing remains a significant challenge. For instance, Sun et al. [22] deployed barometric sensors in a dome-shaped elastomer, achieving super-resolution 3D force sensing through the Taxel Value Isolines (TVIs) theory and a Multilayer Perceptron (MLP) model. However, shear forces introduce a twisting effect on the TVIs, which compromises estimation accuracy. Yan et al. [13] designed a sinusoidally magnetized flexible film where normal and shear force could be decoupled by detecting changes in magnetic flux density using a Hall sensor. A neural network was used to achieve a 60-fold super-resolution accuracy. However, its design can only resolving 2D forces (normal and uniaxial shear), restricting its application in full 3D force perception.

To address these limitations, our design provides a solution for super-resolution 3D force perception. Sensing units positioned at the base of the soft silicone layer directly capture the 3D force components transmitted through the silicone layer, with a hybrid model-learning framework. These signals encode the information necessary to reconstruct both the location and magnitude of the external force. Since silicone is a visco-elastic material whose elastic modulus changes with strain, it is difficult to create an accurate physical model for force measurement [23]. Therefore, we use a learning-based method to train models, enabling super-resolution 3D force sensing.

III. Design of Three-Dimensional Force Sensing Unit

A. Mechanical Design of the Sensing Unit

The proposed tactile sensing unit is designed to achieve three-dimensional force perception while maintaining a compact structure and good scalability. The units are fabricated using a Formlabs Form4 stereolithography (SLA) 3D printer. To facilitate array-level integration, each unit is designed with a small form factor, featuring an overall diameter of 8 mm and a thickness of 4.5 mm. A square protrusion with dimensions of $5 \times 5 \times 1.5$ mm is integrated at the bottom of the unit, allowing it to be inserted into the predefined slot for fixation and positioning, as shown in Fig. 2(a). This design enables flexible installation, easy replacement, and scalable deployment at arbitrary locations. Unlike many existing designs (e.g.,

[24],[25]), which typically employ four cantilevers or piezoresistive modules to achieve three-dimensional force sensing, the proposed unit simplifies the architecture by utilizing only three identical cantilevers. They are symmetrically distributed around the center of the unit with a $120°$ spacing. The compact architecture reduces the number of sensing elements while preserving the capability for three-dimensional force measurement, thereby lowering system complexity and cost. Each cantilever has a width of 1.5 mm and a thickness of 0.3 mm. The selected thickness represents a balanced trade-off between mechanical robustness and sensitivity, as thinner beams are prone to fracture, while thicker ones exhibit insufficient deformation under low-magnitude forces.

The hollow region inside the unit is filled with silicone (Shore 40A), facilitating rapid elastic recovery and ensuring that the cantilevers reliably return to their original positions after unloading. A miniature strain gauge is bonded near the fixed end of each cantilever. Finally, a rigid cylindrical probe ($\phi\, 3 \times 2$ mm) is bonded at the center of the unit to transmit external forces. When an external force is applied to the probe, the resulting deformation produces distinct responses among the three cantilevers, providing the physical basis for 3D force decoupling.

B. Sensing Principle

Each tactile sensing unit employs miniature strain gauges (CY120-1-1MM, size 2.1×1.2 mm) as sensing elements. Rather than measuring force directly, these gauges detect the bending-induced surface strain of the cantilever, which correlates with the applied load. The relationship between the fractional change in resistance and the mechanical strain is expressed as follows:

$$\frac{\Delta R}{R} = G \cdot \varepsilon, \tag{1}$$

where R is the nominal resistance of the strain gauge, ΔR represents the resistance change, G denotes the gauge factor, and ε denotes the mechanical strain at the gauge location.

A dedicated strain acquisition module is employed to quantify the resistance variations and convert them into corresponding strain values. Here, strain (ε) is a dimensionless quantity defined as the relative change in length, reported in microstrain ($\mu\varepsilon$) throughout this work for numerical clarity. Each acquisition channel outputs a digitized $\mu\varepsilon$ value that reflects deformation of the corresponding cantilever, serving as the raw input for subsequent force estimation.

In the proposed structure, external forces applied to the probe are transmitted to the cantilevers, inducing bending deformation. Under the assumptions of infinitesimal deformation and linear elasticity, the normal strain on the cantilever surface can be analytically expressed using the Euler-Bernoulli beam theory:

$$\varepsilon = \frac{My}{EI}, \tag{2}$$

where M is the bending moment acting on the beam, y is the distance from the neutral axis to the strain gauge location, E is the Young's modulus of the beam material, and I denotes the second moment of area of the beam cross-section. For a concentrated force F applied at the free end, the bending moment $M(x)$ satisfies:

$$M(x) = F(L - x), \tag{3}$$

where L denotes the beam length and x is the distance from the fixed end. Since the strain gauges are located at a fixed distance x, the measured strain ε is proportional to the applied force F within the elastic operating range.

C. Model-based and Learning-based Tri-Axial Force Decoupling

After characterizing the force–strain relationship of each cantilever, the probe is bonded at the center of the sensing unit. To validate the tri-axial force perception ability of the sensing unit, Finite Element Analysis (FEA) is conducted to characterize the structural response of the cantilevers under distinct loading conditions, as illustrated in Fig. 2(b)–(d). Under a normal force F_z, all three cantilevers exhibit uniform deformation patterns consistent with the structural symmetry. In contrast, the application of a shear force F_x along the x-axis causes Cantilever 1 to undergo compression while Cantilevers 2 and 3 experience symmetric tensile strain of a smaller magnitude. Furthermore, a force along the y-axis induces a characteristic anti-symmetric deformation in Cantilevers 2 and 3, whereas Cantilever 1 remains stationary along the vertical axis. These simulated responses collectively corroborate the mechanical foundation for decoupling three-dimensional force components within the sensing unit.

To establish the force decoupling model for a single sensing unit, let $\boldsymbol{F}_{unit} = [F_{x,unit}, F_{y,unit}, F_{z,unit}]^\top \in \mathbb{R}^3$ denote the external force vector applied to the rigid probe, and let $\boldsymbol{f} = [f_1, f_2, f_3]^\top \in \mathbb{R}^3$ denote the normal forces detected at the tips of the three cantilevers. When external shear forces are applied to the probe tip, they generate overturning moments proportional to the probe height h (the vertical lever arm). To maintain static equilibrium, these moments are counterbalanced by the vertical reaction forces of the cantilevers acting across the distribution diameter d (the horizontal lever arm). Based on static equilibrium analysis, the mapping between internal measurements and external loads is derived as:

$$\begin{bmatrix} F_{x,unit} \\ F_{y,unit} \\ F_{z,unit} \end{bmatrix} = \begin{bmatrix} -\dfrac{d}{2h} & \dfrac{d}{4h} & \dfrac{d}{4h} \\ 0 & -\dfrac{\sqrt{3}d}{4h} & \dfrac{\sqrt{3}d}{4h} \\ 1 & 1 & 1 \end{bmatrix} \begin{bmatrix} f_1 \\ f_2 \\ f_3 \end{bmatrix}. \tag{4}$$

This linear relationship is formalized as $\boldsymbol{F}_{unit} = \boldsymbol{A}\boldsymbol{f} + \boldsymbol{B}$,where $\boldsymbol{A} \in \mathbb{R}^{3\times 3}$ is the coefficient matrix and $\boldsymbol{B} \in \mathbb{R}^3$ is a constant bias vector. The objective of the decoupling process is to identify $\boldsymbol{A}$ and $\boldsymbol{B}$. Given the linear mapping between $\boldsymbol{F}_{unit}$ and $\boldsymbol{f}$ established through analytical derivation within the elastic range, a Multi-Input Multi-Output (MIMO) least-squares method is employed to estimate parameters $\boldsymbol{A}$ and $\boldsymbol{B}$. Pairs of input data $\boldsymbol{f}$ and output data $\boldsymbol{F}_{unit}$ are collected across diverse loading directions, enabling a robust estimation of the parameters. Notably, the bias term $\boldsymbol{B}$ effectively compensates for system errors even in the presence of minor assembly misalignments.

However, the estimation accuracy of the least-squares model deteriorates under large deviations from the normal direction. To address this, an MLP is introduced to capture non-linearities under large-tilt-angle contacts. Experiments show that the learning-based method outperforms the model-based approach when the contact angle exceeds $40°$. Consequently, a hybrid decoupling strategy is adopted: the least-squares model is utilized for near-normal forces, while the MLP model is activated for force angles surpassing $40°$. This angle-based hybrid strategy ensures robust and accurate tri-axial force estimation across an extended range of loading conditions.

IV. Super-Resolution 3D Force Perception

This section details our super-resolution 3D force perception method, which leverages traction-coupling effects within a compliant silicone layer. Surface loads produce deformations that propagate through the elastomer, generating spatially correlated yet distinguishable responses across multiple underlying units. By mapping these coupled signals to the applied 3D force and contact location, the system achieves continuous localization and high-fidelity force estimation.

A. Tactile Array Design with a Soft Silicone Layer

The tactile array consists of four taxels arranged in a 2×2 configuration with a 13 mm pitch. Each taxel is directly inserted into a slot on a rigid base for fixation and alignment, facilitating easy installation and removal, as shown in Fig. 1(a). In the event that a single taxel fails, the issue can be addressed by replacing only the affected unit rather than the entire tactile array, significantly lowering maintenance costs. The sensing array is covered by a 5-mm thick silicone layer (Shore 20A) acting as a synthetic skin. Rather than transferring loads to a single taxel, the compliant silicone distributes the mechanical stimulus spatially. Beneath this compliant interface, taxels respond with unique magnitudes and directions depending on their orientation and proximity to the contact point. Under consistent boundary conditions, these elastic propagation patterns are repeatable and distinguishable, providing sub-taxel information that allows the effective sensing resolution to exceed the physical taxel density.

For calibration, we define a 13×13 mm sensing array matching the taxel pitch. A local two-dimensional coordinate frame is defined on the silicone surface, with the origin $(0, 0)$ located at the lower-left corner of the array. The array observation $\boldsymbol{x} = [\boldsymbol{F}_{unit,1}^\top, \boldsymbol{F}_{unit,2}^\top, \boldsymbol{F}_{unit,3}^\top, \boldsymbol{F}_{unit,4}^\top]^\top \in \mathbb{R}^{12}$ is formed by concatenating the four taxel outputs. The objective is to infer the external force $\boldsymbol{F}_{ext} = [F_{x,ext}, F_{y,ext}, F_{z,ext}]^\top \in \mathbb{R}^3$ and the continuous contact location $\boldsymbol{p} = [x, y]^\top \in \mathbb{R}^2$ from $\boldsymbol{x}$.

B. Learning-Based Super-Resolution Estimation of 3D Force and Contact Location

Building an accurate analytical model is challenging because silicone exhibits nonlinear behavior, and its force–deformation relationship can vary with loading conditions[23]. Consequently, we adopt a data-driven approach to map the observation vector $\boldsymbol{x}$ to the 3D force $\boldsymbol{F}_{ext}$ and contact location $\boldsymbol{p}$. This work assumes single-contact interactions; for a sparse 2×2 array, multiple simultaneous contacts would superimpose complex coupling patterns, rendering the inverse problem highly ill-posed.

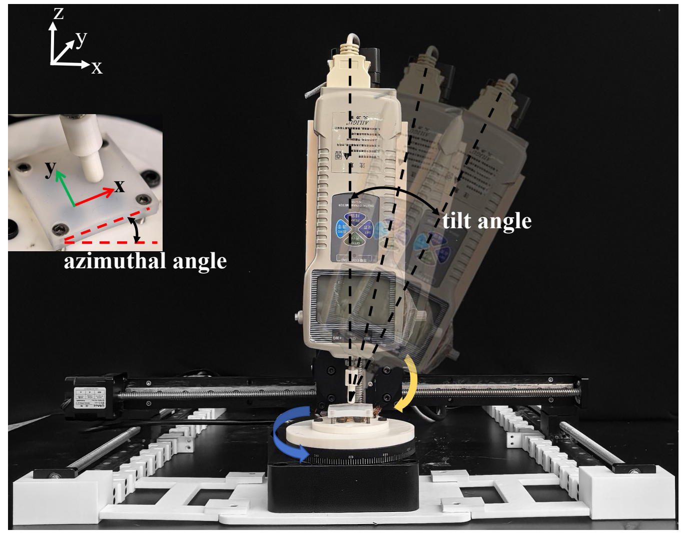

Fig. 3. **Automated calibration platform with 5-DoF.**

To collect high-fidelity training data, an automated calibration platform is developed, as shown in Fig. 3. The tactile array is mounted on a motorized rotary stage to adjust the azimuthal angle β, while a force gauge is controlled by a 3-axis xyz motion system to perform programmable indentation. A tilting mechanism regulates the tilt angle α relative to the global Z-axis. The dataset samples β over the full $360°$ range at $30°$ increments and $\alpha \in \{0°, 15°, 30°\}$; larger tilt angles are excluded to avoid friction-induced slip and ensure repeatability. Using a 6 mm spherical indenter with a 2.6 mm spatial step, we sample 36 locations within a 13×13 mm array. Forces ranging from 0 to 4 N are applied at each location and angle, resulting in approximately 10^5 training samples. The tri-axial ground truth vector $\boldsymbol{F}_{ext}$ is computed by resolving the scalar magnitude from the force gauge via a coordinate transformation based on α and β. Ground truth values for $\boldsymbol{p}$ are derived from commanded coordinates.

To learn the mapping from sensor observations to these ground truth values, the inference model comprises two lightweight MLPs to predict the contact location $\hat{\boldsymbol{p}} = [\hat{x}, \hat{y}]^\top$ and the force vector $\hat{\boldsymbol{F}_{ext}} = [\hat{F}_{x,ext}, \hat{F}_{y,ext}, \hat{F}_{z,ext}]^\top$. The position network features three hidden layers (256, 128, and 64 neurons) to capture complex spatial non-linearities, while the force network utilizes a more compact structure (128, 64, and 32 neurons). Both networks utilize ReLU activations and are trained using Mean Squared Error (MSE) loss with the Adam optimizer. During real-time inference, the system processes $\boldsymbol{x}$ to provide continuous 3D force and location estimation, effectively achieving super-resolution perception beyond the physical taxel spacing.

V. Experiment

In this section, we evaluate the accuracy of the proposed sensing unit and tactile sensor, and further demonstrate their effectiveness in practical manipulation tasks. Specifically, we use the sensing unit to teleoperate a robot arm to insert a test tube into a rack, and mount the tactile sensor onto a robotic gripper to achieve stable ping-pong ball grasping under external disturbances.

A. Sensing Unit Characterization

1) Linearity Validation: We first validate the linear relationship between the cantilever strain ε and the normal force F applied at the free end of the cantilever. After bonding strain gauges to the cantilever, we apply forces in the range of approximately 0–2 N to the beam tip using the setup shown in Fig. 3 with a smaller indenter, while simultaneously recording strain measurements via a strain acquisition module. We then fit the collected data using least-squares regression, resulting in a linear curve shown in Fig. 4, with a coefficient of determination $R^2 = 0.9997$. This excellent linearity substantiates the Euler-Bernoulli beam model and provides a theoretical foundation for 3D force decoupling.

2) Decoupling Strategy Evaluation: To compare the accuracy of model-based, learning-based, and hybrid decoupling strategies, we collected test samples within the measurement range ($F_z < 4$ N and $F_x, F_y < 2$ N) under different force directions and divide them into two groups: angles below $40°$ and above $40°$. As shown in Fig. 5, the model-based method achieves lower MAE in the near-normal region ($< 40°$, 0.37 N vs. 0.55 N), likely because data sparsity hinders the MLP's convergence in this regime. Conversely, the learning-based method outperforms the model-based method in the large-angle regime ($> 40°$, 0.51 N vs. 0.65 N) by capturing non-linearities. Consequently, the proposed hybrid strategy yields the lowest overall MAE (0.46 N), outperforming both the pure model-based (0.55 N) and learning-based (0.53 N) baselines, which verifies the advantage of the proposed hybrid decoupling strategy.

3) Cross-Axis Coupling Evaluation: To characterize the decoupling capability of our sensing unit, we apply forces along three directions: the normal direction and two oblique directions (30° tilt toward the $+x$-axis and the $+y$-axis). The results are shown in Fig. 6, which plots the estimated forces and the ground truth on three axes. For quantitative evaluation, we introduce the single-axis coupling error η_{ij}, defined as the percentage of the maximum spurious force $F_{i,out}$ on an unloaded axis (i) relative to its full-scale capacity $F_{i,F.S.}$ when a load is applied on the loaded axis (j). The metric is computed as follows:

$$\eta_{ij} = \frac{|F_{i,out}|}{F_{i,F.S.}} \times 100\%, \quad (i \neq j), \tag{5}$$

Lower η_{ij} indicates better decoupling performance. The maximum coupling error of our sensing unit is 10.8%, confirming its strong decoupling capability.

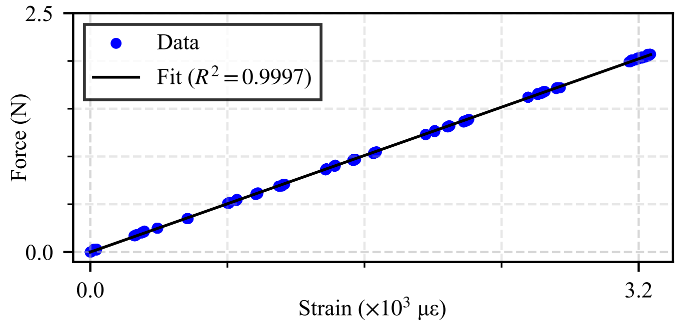

Fig. 4. **Relationship between the force on the beam tip and the microstrain.** We fit the data using linear least-squares regression, yielding a coefficient of determination $R^2 = 0.9997$.

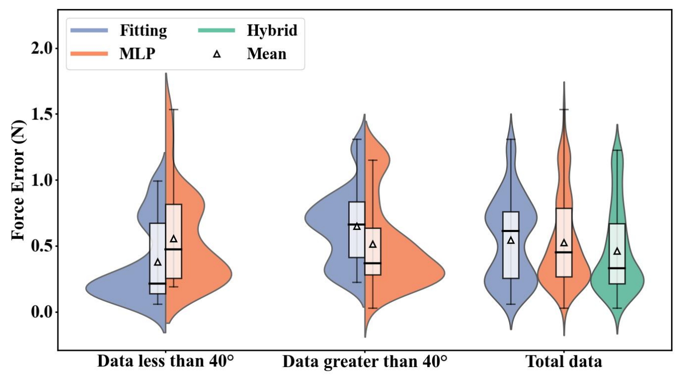

Fig. 5. **Statistical comparison of force estimation errors across different decoupling strategies and angle data.** The left and middle panels compare the Least-Squares Fitting (blue) and MLP (orange) methods under distinct angle intervals. The right panel evaluates all three methods (including the proposed hybrid strategy in green) on the total dataset, demonstrating that the hybrid strategy achieves the lowest overall error.

B. Tactile Sensor Evaluation

1) Super-Resolution Accuracy Evaluation: To rigorously evaluate the accuracy of the proposed array-based tactile sensor, we conduct dense sampling at 1 mm intervals across the sensor surface rather than relying solely on held-out test sets, recording the applied 3D force and position ground truth alongside the corresponding sensor estimates. Fig. 7(a) and (b) visualizes the spatial distributions of force and position errors, respectively. The system achieves an MAE of 0.19 N for 3D force estimation and 0.49 mm for localization. Evaluations using a densely sampled dataset demonstrate an approximate 3 times enhancement in super-resolution capability, as detailed in the supplementary material.

2) Model Transferability Evaluation: We further test an alternative end-to-end model using the same MLP architecture but replacing the inputs with the raw loads measured on the 12 cantilevers (from four sensing units), skipping the intermediate unit-level decoupling. This approach is expected to be more accurate in principle, and indeed achieves a lower errors (Force MAE: 0.14 N, Location MAE: 0.41 mm). Nevertheless, we still adopt the hierarchical approach—using decoupled unit forces as inputs—that learns the mapping from

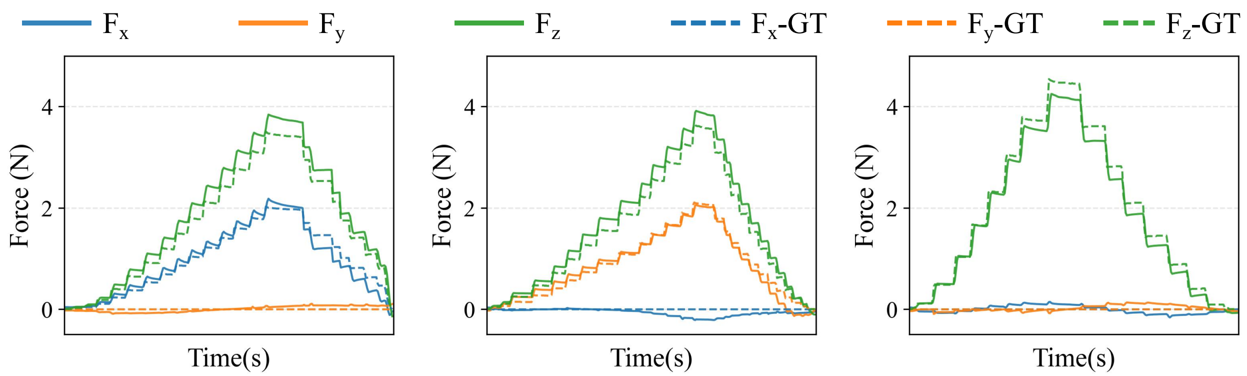

Fig. 6. **Validation of 3D force tracking and decoupling performance under dynamic staircase loading.** The solid lines represent the sensor estimates, while the dashed lines denote the ground truth (GT). Left: Oblique loading (30° tilt toward the $+x$-axis). Middle: Oblique loading (30° tilt toward the $+y$-axis). Right: Pure normal loading.

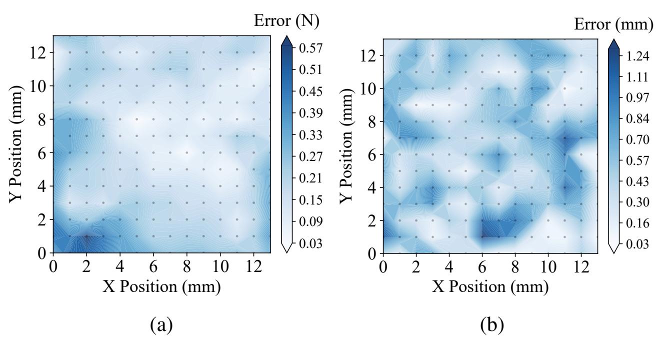

Fig. 7. **Spatial distribution of estimation errors across the effective sensing area (13×13 mm).** The discrete black dots indicate the evaluation locations. (a) 3D force estimation error (N). (b) Contact localization error (mm).

TABLE I
PERFORMANCE COMPARISON BETWEEN DIFFERENT HIERARCHICAL AND END-TO-END MODELS.

Models	**Location MAE (mm)**	**Force MAE (N)**
Hierarchical	**0.49**	**0.19**
End-to-end	0.41	0.14
Transferred hierarchical	1.22	0.32
Transferred end-to-end	1.73	0.44

contact forces to force responses at four fixed unit points. This choice enables modular replacement: a faulty sensing unit can be replaced without retraining the global model. To validate this, we deploy both models on a newly fabricated sensor array and evaluate the MAE shown in Table I. The end-to-end model exhibits larger errors than our hierarchical model in newly fabricated tactile sensor. Therefore, our design avoids repeated data collection and retraining in future deployments, facilitating large-area super-resolution 3D force sensing.

C. Robotic Manipulation Demonstrations

Following the static characterization, we validate the proposed sensor in dynamic interaction scenarios through two distinct manipulation experiments: (1) high-precision teleoperation using the sensing unit, and (2) closed-loop adaptive grasping using the tactile sensor under external disturbances.

1) Precision Teleoperation: To demonstrate the sensing unit's force decoupling capability and practical potential, we teleoperated a robot arm using the sensing unit to insert a test tube (ϕ 28.5 mm) into a tube rack (ϕ 30 mm), as shown in Fig. 8. Leveraging its compact form factor, we utilized the sensing unit as a fingertip miniature joystick that accurately captures 3D forces applied by the user. A simple control algorithm converts the sensed forces into motion commands along the six cardinal translational directions ($\pm x, \pm y, \pm z$) of the robot. The commands are streamed to the robot controller in real time, driving the robot with a fixed step size. Despite the tight clearance (1.5 mm), the task is completed smoothly. This result demonstrates the sensing unit's effective force decoupling capability.

2) Disturbance-Robust Adaptive Grasping: To further explore the potential of the tactile sensor for dexterous grasping, we conduct an experiment where a robotic gripper, equipped with the proposed tactile sensor, stably grasps a ping-pong ball under external disturbances. Conventional grippers often lack shear-force sensing at the contact interface, leading to limited adaptability during grasping. We implement a complete experimental pipeline consisting of "steady grasping—slip prediction and suppression—human-in-the-loop release". The experiment aims to demonstrate that the proposed sensor can accurately monitor both normal gripping forces (F_z) and tangential friction forces (F_y) enabling robust grasping, while also detecting pulling forces along the x-direction to infer the operator's intention to retrieve the object.

As shown in Fig. 9, the tactile sensor is mounted on a gripper (Robotiq 2F-85). During Phase I (0-t_1), when the gripper is not in contact with any object, the measured forces along the three axes remain near 0 N. At t_1, a ping-pong ball is placed at a predefined location and the gripper closes with an initial normal grasping force of F_z (0.86 N). The extremely light weight of the ball (2.7 g) results in negligible force along the y-axis. Subsequently, an external downward pulling force is applied to extract the ball, gradually increasing its magnitude. At t_2, the system computes a slip ratio $-F_y/F_z$

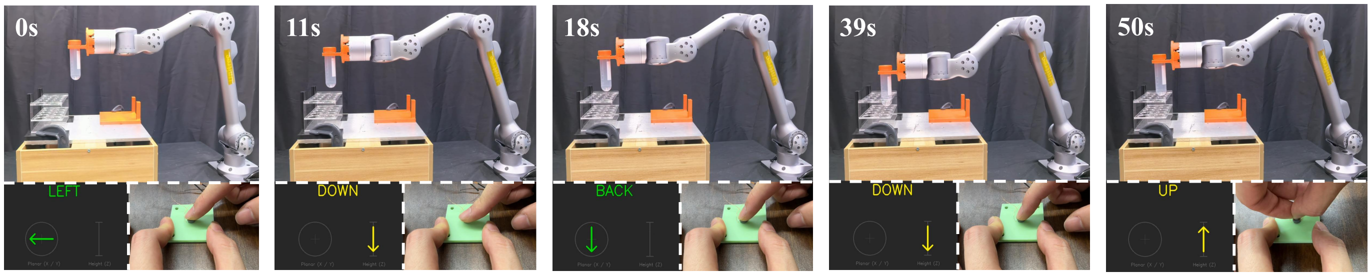

Fig. 8. **Demonstration of a teleoperated peg-in-hole task using a single sensing unit.** The operator applies 3D forces on the sensor surface, which are mapped to the robotic arm's translational motion along three axes, successfully inserting the test tube into the rack. The insets display the physical interaction between the operator and the sensor (bottom right) and the corresponding real-time motion commands derived from the decoupled 3D force vector (bottom left).

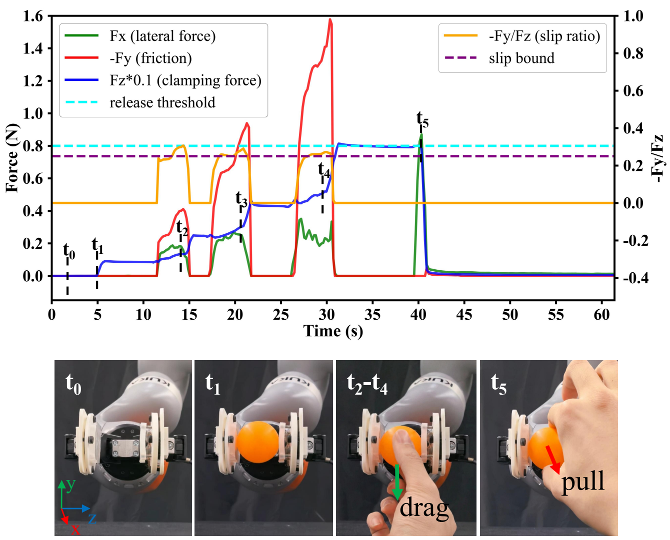

Fig. 9. **Experimental validation of disturbance-robust adaptive grasping and intention-aware release** Top: Real-time evolution of contact forces and slip ratio. The blue line represents the clamping force (F_z, scaled by 0.1), while the red and green lines denote tangential friction ($-F_y$) and lateral interaction force (F_x), respectively. Bottom: Snapshots of key events. At t_0, the sensor is in a static unloaded state on the open gripper. At t_1, the object is grasped. From t_2 to t_4, external downward disturbances cause the slip ratio (yellow line) to intermittently exceed the slip bound (0.25, purple dashed line), triggering an adaptive increase in F_z to suppress slip. At t_5, a lateral pull is detected; once F_x surpasses the release threshold (0.8 N, cyan dashed line), the system identifies the retrieval intention and releases the object.

that exceeds the slip bound (0.25, based on the contact friction coefficient). In response, the controller tightens the grasp, resulting in the grasping force increasing to 2.5 N. Notably, due to misalignment between the applied disturbance and the y-axis, a response is also observed along the x-axis. During Phase II (t_2-t_3), we first remove the pulling force and monitor F_x and F_y, which both return to approximately 0 N, confirming low cross-axis coupling and robust decoupling performance. The pulling force is reapplied until t_3, at which point the slip ratio again exceeds the threshold, prompting the gripper to increase the grasping force to 4.3 N. This process is repeated in subsequent cycles.

At t_5, we apply a lateral force F_x to intentionally retrieve the ball. The tactile sensor detects an increase in lateral force (F_x) to 0.87 N, which exceeds the release threshold (0.8 N), causing the gripper to open and release the object, successfully completing the retrieval. In comparison, under the same experimental conditions, a baseline without tactile-feedback control results in the ball slipping and dropping at approximately 10 s, as shown in movie S3. These results highlight the critical role of the 3D tactile force sensor in ensuring disturbance-robust and stable grasping. Additionally, more experiments validating the sensor's practicality in manipulation tasks are provided in the supplementary material.

VI. Conclusion

In this paper, we presented a super-resolution tactile sensor capable of precise three-dimensional force perception. The design integrates a soft artificial skin with a sparse array of monolithic tri-cantilever sensing units, mimicking the structure and function of human mechanoreceptors. By employing a hybrid model-learning decoupling strategy at the unit level and leveraging deep learning to interpret traction-coupling effects at the array level, the proposed sensor achieves accurate reconstruction of external stimuli. Experimental results demonstrate that our system attains a force estimation MAE of 0.19 N and a localization MAE of 0.49 mm, representing a 26-fold improvement in spatial resolution beyond the physical taxel density. Furthermore, the adoption of a hierarchical modeling approach ensures excellent transferability, allowing for modular maintenance without the need for global retraining. The practical utility and robustness of the sensor were successfully validated through high-precision teleoperation and disturbance-adaptive grasping tasks.

Building upon the inherent scalability and modularity of our design, future work will focus on two primary directions. First, leveraging the modularity and scalability of our design, we aim to expand the tactile array to cover larger surface areas, specifically targeting integration onto robotic hands and arms. Second, we plan to adapt the sensor design for deployment on curved surfaces, thereby enabling better conformity to complex geometries.

Acknowledgments

This work is supported by the Open Competition Mechanism on Humanoid Robot of Longyou County, Zhejiang

Province, Major Scientific and Technological Research Project under Grant 2025246, the Independent Project of State Key Laboratory of Industrial Control Technology under Grant ICT2025A06, the Special Fund for Innovation and Development of Hangzhou West Science and Technology Innovation Corridor under Grant K-20241950.

REFERENCES

[1] Ganna Pugach, Artem Melnyk, Olga Tolochko, Alexandre Pitti, and Philippe Gaussier. Touch-based admittance control of a robotic arm using neural learning of an artificial skin. In *2016 IEEE/RSJ International Conference on Intelligent Robots and Systems (IROS)*, pages 3374–3380. IEEE, 2016.

[2] Shoujie Li, Tong Wu, Jianle Xu, Yan Huang, Zongwen Zhang, Hongfa Zhao, Qinghao Xu, Zihan Wang, Linqi Ye, Yang Yang, et al. Biomimetic multimodal tactile sensing enables human-like robotic perception. *Nature Sensors*, 1(1):52–62, 2026.

[3] Liang Zou, Chang Ge, Z Jane Wang, Edmond Cretu, and Xiaoou Li. Novel tactile sensor technology and smart tactile sensing systems: A review. *Sensors*, 17(11):2653, 2017.

[4] Shaoxiong Wang, Jiajun Wu, Xingyuan Sun, Wenzhen Yuan, William T Freeman, Joshua B Tenenbaum, and Edward H Adelson. 3d shape perception from monocular vision, touch, and shape priors. In *2018 IEEE/RSJ International Conference on Intelligent Robots and Systems (IROS)*, pages 1606–1613. IEEE, 2018.

[5] Chaofan Zhang, Shaowei Cui, Shuo Wang, Jingyi Hu, Yinghao Cai, Rui Wang, and Yu Wang. Gelstereo 2.0: An improved gelstereo sensor with multimedium refractive stereo calibration. *IEEE Transactions on Industrial Electronics*, 71(7):7452–7462, 2023.

[6] Jing Xu, Weihang Chen, Hongyu Qian, Dan Wu, and Rui Chen. ThinTact: Thin Vision-Based Tactile Sensor by Lensless Imaging. *IEEE Transactions on Robotics*, 2025.

[7] A Iggo and Ao R Muir. The structure and function of a slowly adapting touch corpuscle in hairy skin. *The Journal of physiology*, 200(3):763, 1969.

[8] Kenneth O Johnson. The roles and functions of cutaneous mechanoreceptors. *Current opinion in neurobiology*, 11 (4):455–461, 2001.

[9] Tatiana Kardashina. Review of mechanoreceptors and the neural processing of touch sensations. 2025.

[10] Huanbo Sun and Georg Martius. Guiding the design of superresolution tactile skins with taxel value isolines theory. *Science Robotics*, 7(63):eabm0608, 2022.

[11] Jian Hou, Xin Zhou, and Adam Spiers. Location and orientation super-resolution sensing with a cost-efficient and repairable barometric tactile sensor. *IEEE Transactions on Robotics*, 41:729–741, 2024.

[12] Zhou Lu, Yuan Su, Qi Ye, Ze Wang, Xiufang Shi, Gaofeng Li, and Jiming Chen. A low-cost super-resolution tactile sensor: design, fabrication and validation. *IEEE Sensors Journal*, 2024.

[13] Youcan Yan, Zhe Hu, Zhengbao Yang, Wenzhen Yuan, Chaoyang Song, Jia Pan, and Yajing Shen. Soft magnetic skin for super-resolution tactile sensing with force self-decoupling. *Science Robotics*, 6(51):eabc8801, 2021.

[14] Yuhao Sun, Ning Cheng, Shixin Zhang, Wenzhuang Li, Lingyue Yang, Shaowei Cui, Huaping Liu, Fuchun Sun, Jianwei Zhang, Di Guo, et al. Tactile data generation and applications based on visuo-tactile sensors: A review. *Information Fusion*, 121:103162, 2025.

[15] Wenzhen Yuan, Siyuan Dong, and Edward H Adelson. Gelsight: High-resolution robot tactile sensors for estimating geometry and force. *Sensors*, 17(12):2762, 2017.

[16] Chaofan Zhang, Shaowei Cui, Jingyi Hu, Tianyu Jiang, Tiandong Zhang, Rui Wang, and Shuo Wang. TacFlex: Multi-Mode Tactile Imprints Simulation for Visuotactile Sensors with Coating Patterns. *IEEE Transactions on Robotics*, 2025.

[17] Zhenxuan Zhao, Jianshi Tang, Jian Yuan, Yijun Li, Yuan Dai, Jian Yao, Qingtian Zhang, Sanchuan Ding, Tingyu Li, Ruirui Zhang, et al. Large-scale integrated flexible tactile sensor array for sensitive smart robotic touch. *ACS nano*, 16(10):16784–16795, 2022.

[18] Yancheng Wang, Xin Wu, Deqing Mei, Lingfeng Zhu, and Jianing Chen. Flexible tactile sensor array for distributed tactile sensing and slip detection in robotic hand grasping. *Sensors and Actuators A: Physical*, 297: 111512, 2019.

[19] Depeng Kong, Yuyao Lu, Shuyao Zhou, Mengke Wang, Gaoyang Pang, Baocheng Wang, Lipeng Chen, Xiaoyan Huang, Honghao Lyu, Kaichen Xu, et al. Super-resolution tactile sensor arrays with sparse units enabled by deep learning. *Science Advances*, 11(27):eadv2124, 2025.

[20] De Clercq Thomas, Anatolii Sianov, and Guillaume Crevecoeur. A soft barometric tactile sensor to simultaneously localize contact and estimate normal force with validation to detect slip in a robotic gripper. *IEEE Robotics and Automation Letters*, 7(4):11767–11774, 2022.

[21] Jinghui Wang, Xiaoyu Liu, Yujiao Du, Yepu Chen, Jieyi Guo, Linyuan Fan, Min Tang, Xiaofeng Qiao, Yuanjie Zhu, Zhiyang Zhang, et al. A Tangentially Sensitive Tactile Sensor Reveals the Stick-Slip Mechanism and Enhances Robotic Tactile Sensing. *Advanced Science*, page e17884, 2025.

[22] Huanbo Sun, Adam Spiers, Hyosang Lee, Jonathan Fiene, and Georg Martius. Sensing multi-directional forces at superresolution using taxel value isoline theory. *Nature Communications*, 16(1):8031, 2025.

[23] Fellner Schneider, T Fellner, J Wilde, and U Wallrabe. Mechanical properties of silicones for MEMS. *Journal of Micromechanics and Microengineering*, 18(6):065008, 2008.

[24] Dongsheng Li, Aomen Li, Zhongbin Zhang, Tianci Ji, Kaiyao Wang, and Huicong Liu. Highly sensitive MEMS

three-dimensional force sensor for robot-assisted minimally invasive surgery. *Science China Technological Sciences*, 68(9):1920301, 2025.

[25] Ye Qiu, Fangnan Wang, Zhuang Zhang, Kuanqiang Shi, Yi Song, Jiutian Lu, Minjia Xu, Mengyuan Qian, Wenan Zhang, Jixuan Wu, et al. Quantitative softness and texture bimodal haptic sensors for robotic clinical feature identification and intelligent picking. *Science Advances*, 10(30):eadp0348, 2024.